The Linnean Society of London
ZOOLOGICAL Journal of the Linnean Society

A redescription of the skull of the Australian flatback sea turtles *Natator depressus*, provides new morphological evidence for the phylogenetic relationships among sea turtles (Chelonioidea)

Journal:	*Zoological Journal of the Linnean Society*
Manuscript ID	ZOJ-12-2019-3942.R3
Manuscript Type:	Original Article
Keywords:	comparative anatomy < Anatomy, computed tomography < Anatomy, cranium < Anatomy, skull < Anatomy, mandible < Anatomy, Bayesian analysis < Phylogenetics, Chelonia < Taxa
Abstract:	Chelonioidea (sea turtles) are a group where available morphological evidence for crown group relationships are incongruent with those established using molecular data. However, morphological surveys of crown group taxa tend to focus on a recurring subset of the extant species. The Australian flatback sea turtle, *Natator depressus*, is often excluded from comparisons and it is the most poorly known of the seven extant species of Chelonioidea. Previous descriptions of its skull morphology are limited and conflict. Here we describe three skulls of adult *N. depressus* and re-examine the phylogenetic relationships according to morphological character data. Using X-ray micro Computed Tomography we describe internal structures of the braincase and identify new phylogenetically informative characters not previously reported. Phylogenetic analysis using a Bayesian approach strongly supports a sister group relationship between *Chelonia mydas* and *N. depressus*, a topology which wasn't supported by previous analyses of morphological data but one that matches the topology supported by analysis of molecular data. Our results highlight the general need to sample the morphological anatomy of crown group taxa more thoroughly before concluding that morphological and molecular evidence is incongruous.

INTRODUCTION

Analysis of molecular data is the most common way to infer the phylogenetic relationships of modern groups due to numerous inherent advantages (San Mauro and Agorreta 2010; McCormack and Faircloth 2013) but morphology is still important. Firstly, understanding the morphology of modern groups is key to understanding their functional anatomy and character assembly (e.g. Jones et al. 2012; Cordero et al. 2018). Secondly, morphology still has a crucial role within phylogenetic analyses because it allows inclusion of fossil material (Donoghue *et al*. 1989; Ronquist *et al*. 2012; Schnitzler *et al* 2017; Lee and Yates 2018). Moreover, re-examination of the morphology of extant taxa has the potential to generate new phylogenetic characters and new insights into their origins. Re-examinations of morphology in a variety of groups have identified morphological characters that support relationships previously only supported by molecular data (Shaffer *et al.* 1997; Lee 2001; Geisler and Uhen 2003; Asher and Lehmann, 2008; Asher *et al.* 2008; Legg *et al.* 2013). Modern application of morphological data can also help resolve or improve support for relationships that were otherwise contentious based on molecular data alone (Gatsey *et al.* 2003; Lee 2009; Springer *et al.* 2015).

Sea turtles (from here defined as Chelonioidea as defined by Evers *et. al* (2019) are a well-studied group of reptiles that represent the only surviving clade of Mesozoic marine reptiles. There are seven living species, *Caretta caretta* (Linnaeus 1758), *Chelonia mydas* (Linnaeus 1758), *Eretmochelys imbricata* (Linnaeus 1766), *Lepidochelys olivacea* (Eschscholtz 1829), *Lepidochelys kempii* (Garman 1880), *Natator depressus* (Garmon 1880), and *Dermochelys coriacea* (Blainville 1816). All are large or very large in size (35 kg – 650 kg, Pritchard and Trebbau 1984) and currently regarded as endangered or vulnerable to becoming so (Wyneken and Witherington 2001; Seminoff 2004; Mortimer and Donnelly 2008; Abreu-Grobois and Plotkin 2008; Wallace *et al.* 2013; Casale and Tucker 2017; Wibbels and Tucker 2019). Members of Chelonioidea are characterised by several adaptations to a completely marine lifestyle, i.e. flippers, lack of ability to retract their heads or limbs into their shell, and salt glands (Pritchard and Trebbau 1984; Wyneken and Witherington 2001, Jones *et al.* 2012). Most extant species

have a near global distribution, largely centred in the tropics, although *D. coriacea* has been found as far north as the Arctic Ocean (Willgohs 1957).

The phylogenetic relationships among living sea turtles has reached a consensus based on DNA evidence (Fig. 1; Naro-Maciel *et al.* 2008; Duchene *et al*. 2012; Crawford *et al.* 2015). The deepest division is between *D*. *coriacea* (family Dermochelyidae) and all other sea turtles (family Cheloniidae). Within Cheloniidae there are two clades: one comprising *Natator depressus* + *Chelonia mydas* and another comprising *Eretmochelys imbricata* + Carettini (*C*. *caretta*, *L*. *olivacea* + *L*. *kempii*). Although these relationships are now considered well established the same branching topology has not been recovered using solely morphological data (Zangerl *et al.* 1988; Hirayama 1994; Parham and Fastovsky 1997; Scavezzoni and Fischer 2018). However, the lack of support from morphological characters may not be related to an inherent problem with morphological data. It may instead be a sign that our understanding of sea turtle morphology needs improvement.

Of the six species within Cheloniidae, *Natator depressus* is exceptional with respect to its ecology and life habits. *N. depressus* is the most geographically limited modern sea turtle, being confined to the northern and western Australian continental shelf (Limpus 2007). The clutch size of *N. depressus* is on average about half of that found in other species (Pritchard and Trebbau 1987; Limpus 2007), and the hatchlings are up to 20% larger (Limpus 2007). Uniquely amongst sea turtles *N. depressus* does not migrate to pelagic environments in early life, instead remaining in shallow coastal waters (Limpus *et al.* 1983; Walker and Parmenter 1990; Buskirk and Crowder 1994). Available but limited ecological data suggests it has a broad diet. Recorded stomach contents include largely soft bodied invertebrates, but also corals and molluscs (Bjorndal 1985; Bjorndal *et al.* 1997).

Morphological descriptions of *Natator depressus* that are available (Limpus *et al.* 1988; Zangerl *et al.* 1988, Hirayama 1994) lack detail or describe an immature specimen (Fry 1913) and have been of limited use for determining relationships. Comparative studies by Gaffney (1979), Wyneken (2001) and Jones *et al.* (2012) essentially reported that the skull of *N. depressus* was superficially similar to that of *Lepidochelys olivacea* and to a lesser extent *Ch. mydas*. The paucity of data has led to a confused

taxonomic and phylogenetic history for this species. For much of the Twentieth Century a close relationship between *N. depressus* and *C. mydas* had been accepted due to a few external similarities, e.g. scalation, carapace shape, and flipper length, and *N. depressus* was therefore considered to be a species of *Chelonia* (Baur 1890; Fry 1913; Williams *et al* 1967). However, this arrangement was largely rejected after more quantitative methods failed to support it (Limpus *et al.* 1988, Hirayama 1994). Zangerl *et al.* (1988) and Limpus *et al.* (1988) re-established *N. depressus* in its own genus.

Since the late 1980's, phylogenetic studies have placed *N. depressus* within Cheloniidae in a variety of positions. These include a position as the least nested taxon (Hirayama 1994; Lynch and Parham 2003) or as more closely aligned with the Carettini (Dutton 1996), or with a sister relationship to the Mio–Pliocene sea turtle *Syllomus aegyptiacus* (Lynch and Parham 2003, Parham and Pyenson 2010). In the morphology-only study by Scavezzoni and Fischer (2018) *N. depressus* was found to be in a large polytomy with other chelonids, and not in a clade containg solely the crown. Some studies of sea turtle relationships omitted *N. depressus* altogether (e.g. Gaffney and Meylan 1988; Hirayama 1998; Kear and Lee 2006). Other studies that have included *N. depressus* were not aimed at testing relationships among the living species, and simply used it as part of a backbone constraint (see Parham and Pyenson 2010; Cadena and Parham 2015; Gentry 2017; Evers and Benson 2019; Evers *et al.* 2019; Gentry *et al.* 2019). To date, none of the phylogenetic analyses using morphological characters has recovered *N. depressus* as the sister taxon to *C. mydas* in agreement with DNA sequence analyses without using a constraint based on the molecular data (Naro-Maciel *et al.* 2008; Duchene *et al.* 2012).

The lack of a sufficiently detailed adult skull description for the *N. depressus* is problematic for several reasons. Cranial osteology is an important source of characters for phylogenetics and taxonomy as well as informative for the interpretations of function and ecological habits (Emmerson and Bramble 1993; Hanken and Thorogood 1993; Benton 2008; Parhamn and Pyenson 2010; Watanabe and Slice 2014; Ferreira *et al.* 2016; Evers *et al.* 2019). A full understanding of the cranial osteology of living species is valuable for phylogenetic analyses of the extensive turtle fossil record particularly given that among turtles the skull has the most phylogenetic characters of any single region (Hirayama 1998;

Parham and Pyenson 2010; Candina and Parham 2015; Weems and Brown 2017; Evers and Benson 2019). The skull houses the brain, eyes, and nasal cavity, jaw muscles, as well as the mouth and pharynx (e.g. Paulina-Carabajal 2019; Evers *et al*. 2019), therefore its morphology is intimately related to many aspects of its lifestyle.

Here we redescribe the skull of *N. depressus* in detail and identify ten new osteological characters. We test the phylogenetic utility of these characters, and their effects on the placement of *N. depressus* within the cheloniid phylogenetic tree. Using our new data and including some of the more well-preserved/characterized fossil chelonioids, we re-examine the robustness of morphological data in determining relationships among sea turtles, and the degree of concordance between the new morphological data set and existing molecular data sets.

Institutional Abbreviations

AM: Australian Museum; NHMUK: The Natural History Museum UK; SAMA: South Australian Museum; SMNS; Staatliches Museum für Naturkunde, Stuttgart; WAM; Western Australian Museum; QM: Queensland Museum.

MATERIALS AND METHODS

Three specimens of *Natator depressus* were used, two dry skulls WAM R112123 and WAM R61349, and an unregistered wet specimen (Ethanol preserved head) from Queensland Museum. It should be noted that WAM R61349 has a cranial abnormality: a broad bulge or convexity that involves the posterior portion of both parietals. The two parietals rise dramatically medially towards the supraoccipital. The deformity is larger on the left parietal but the arc across the risen area is smooth suggesting it is a singular deformity rather than a deformity arising on each parietal independently.

The skulls of four other sea turtle species were used for comparison *Chelonia mydas* (SAMA unregistered, NHMUK1967.776c), *Caretta caretta* (SAMA R33830; SAMA Unregistered), *Eretmochelys*

imbricata (WAM 120113, AM J51134), and *Lepidochelys olivacea* (SAMA BM670, SMNS 11070). All specimens used were mature individuals, with skulls that are within the size range reported for adults (Gaffney 1979; Pritchard and Trebbau 1984; Dodd 1988; Zangerl *et al.* 1988; Nishizawa *et al.* 2010). The skulls were examined using classical comparative methods and measured using digital callipers and rulers. Each skull was also subject to X-ray micro computed tomography (CT). This approach enabled generation of digital three-dimensional models that facilitate further examination and description of internal structures and contacts without the need for destructive methods such as disarticulation. Six of the specimens (not SMNS 11070 and NHMUK1967.776c) were scanned at Sound Radiology, Adelaide with a Phillips Ingenuity Core 128 scanner. The voxels were non cubic, with voxel sizes of between 170 and 210 microns in the X and Y axis and 333 microns on the Z axis (See Sup. Table 1). Specimen NHMUK1969.776c was scanned with the Nikon Metrology HMX ST 225. Segmentation and processing was executed in Avizo 8.0 Lite (FEI, Hillboro, Oregon, USA). Specimen SMNS 11070 (*Lepidochelys olivacea*) was downloaded from morphosource to provide additional CT scan data on this species. These specimen models are available for examination and download on morphosource (LINK TO BE CONFIRMED UPON ACCEPTENCE)

The anatomical terminology used largely follows Gaffney (1972). When referring to a structure not referred to in Gaffney (1972), terminology follows Evers *et. al* (2019).

Phylogenetic analysis

Our phylogenetic analysis took the data of Evers and Benson (2019) as its starting point. For our initial data set (data set A) we used a modified set of 23 taxa and 358 morphological characters, focusing on Pan-Chelonioidea, adding some taxa and modifying some characters using information from personal observation, and data from the literature (Appendix 2). We then created a second data set (data set B) by augmenting this modified Evers and Benson set with 10 new characters taken from the present study.

In both the A and B data sets, *Apalone spinifera* was used as an out group, representing the Trionychidae, which are sister to the rest of crown Cryptodira (Crawford *et al.* 2015). *Chelydra serpentina* was used as a representative of Chelydridae, usually found as part of a sister clade to Pan-

Chelonioidea within Americhelydia (Crawford *et al.* 2015; Cardeni and Parham 2015; Evers and Benson 2019). We assumed that the family Protostegidae was part of Cryptodira because almost all studies find them closely aligned with Chelonioidea (Hirayama 1994; Kear and Lee 2006; Cadena and Parham 2015; Evers and Benson 2019 Raselli 2018). The protostegids included were *Rhinochelys pulchriceps, Protostega gigas, Santanchelys gaffneyi,* and *Bouliachelys suteri.* These were chosen to represent the greatest spread of taxa, both chronologically and taxonomically. Several additional species were added that were not present in Evers and Benson 2019. Characters for these species came from their descriptive literature and Cadena and Parham (2015). These species, *Syllomus aegyptiacus* (Weems 1980; Hasegawa *et al.* 2005), *Pacifichelys hutchisoni*(Lynch and Parham 2003; Parham and Pyenson 2010), *Carolinachelys winsonii* (Weems and Sanders 2014; Weems and Brown 2017), and *Procolpochelys grandaeva* (Weems and Sanders 2014; Weems and Brown 2017) were added to better represent the Cenozoic diversity of sea turtles.

To test the validity of our taxon datasets (A and B), set we used two further datasets that included all the taxa previously used in Evers *et al.* (2019) with (D) and without the new characters (C). For D, the new characters were marked as unknown for the taxa not present in A or B. For these datasets *Proganochelys quenstedti* was used as the outgroup as the earliest occurring testudine in Evers and Benson (2019).

We employed a Bayesian analysis using Mr Bayes V 3.2.6. For rate variation, we used a Mkv model with ascertainment correction bias (Lewis 2001), as it is the most thoroughly tested model for incorporating morphological data within a Bayesian framework (Müller and Reisz 2005; Wiens 2009; Pyron 2011). The gamma parameter was chosen to allow for rate variation across characters, as a more realistic option when compared to a uniform rate variation (Nylander *et al.* 2004; Müller *et al.* 2006; Lee 2013). The Bayesian analyses ran for 30,000,000 generations, with a sample frequency of 1000. Parameters, posterior probabilities, and branch lengths were estimated using a Markov chain Monte Carlo, with four chains used, one cold, three heated with a temperature of 0.2. The first 25% of samples were discarded as burn in.

RESULTS

The skull of *Natator depressus* is similar to that of other sea turtles in having a dome shaped cranium that tapers anteriorly and possesses relatively small posterodorsal and ventrolateral emarginations compared to many other Testudines (Fig. 2-5; Jones *et al*. 2012; Foth et al. 2019). The orbits are large (roughly a third the length of the cranium), and the rostrum is short and blunt. The skull in general shape has a shallow profile, a broad posterior region of the skull, and a V shaped lower jaw (Fig. 6,7). The secondary palate is well developed and has two distinct ridges that run parallel to the outer margin of the upper jaw and complement the two ridges on the lower jaw (Fig. 4). The palate is comparatively wide in comparison to other cheloniids.

Upper jaw and palate

The premaxillae are narrow and tall, contributing to the deep profile of the upper jaw. They contact the maxilla along the entirety of the lateral edge, and also posterolaterally via a shelf which also contacts the anterior end of the vomer (Fig. 4). There is a premaxillary pit as seen in other species (Pritchard and Trebbau 1984, SAMA 33830, Unregistered, BM670). The maxilla is relatively deep and fairly robust (Fig. 2.). The maxilla contacts the jugal posteriorly, the external seam for the two bones is sigmoid in lateral view and continues ventrally where it runs anteromedially on the surface of the palate (Fig. 4). In lateral view, the anterior most portion of the maxilla extends posteriorly along the ventral margin of the jugal. This arrangement is also in contrast to the figures shown in Zangerl (1988), where the ventral margin of the maxilla and jugal are largely continuous. The difference in the latter may be due to the angle of view, or perhaps damage to the specimen.

The palatal surface of the maxilla is marked by a prominent ridge that runs parallel to the suture of the palatine and reaches its peak height close to the contact with the vomer (Fig. 4). This ridge corresponds to a ridge on the upper beak. The maxilla contacts the vomer and palatine medially.

The vomer is divided into a ventral portion and dorsal portion separated by a relatively thin midline beam, the vomerine pillar, which also divides the two internal nares. The ventral portion of the vomer, as exposed in ventral view is roughly rectangular and forms the centre of the secondary palate, bounded by both maxillae, palatines, and the premaxillae. The dorsal portion of the vomer forms part of the margin of the *fossa nasalis* and *foramen orbito-nasale.* The premaxilla contacts the vomer dorsally and forms the anteroventral portion of the *fossa nasalis*. Posteriorly the central portion of the vomer is "I" shaped in coronal section (Fig. 8B) but anteriorly it becomes "X" shaped (Fig. 8C). The dorsal prongs of the X contact the prefrontals, whereas the ventral prongs contact the maxillae, the lateral face of the vomer forming the medial face of the *foramen orbito-nasale.* The foramen penetrates the medial and dorsomedial face of the internal nares. The vomer, the palatine, and the maxillae together form the secondary palate, and the triturating surface.

The palatine overlaps the dorsomedial surface of maxilla along its lateral edge, contacts the pterygoid and jugal posteriorly, and contacts the vomer medially above and below the internal naris. The pterygoid contacts the palatine anteriorly, the basisphenoid and exoccipital posteromedially, and the quadrate posteriorly. The pterygoid of *N. depressus* has prominent lateral projections. The posterior half of the pterygoid is significantly thicker than the flat anterior portion. The posterior section of the dorsal surface of the pterygoid provides most of the floor of the *fenestra postoticus*. The *foramen posterius canalis cartotici interni* is prominent at the posterior margin of each pterygoid (Fig. 5). Part of the dorsal margin is formed by the exoccipital (but see Zangerl *et al.* 1988: Fig. 8). The canal runs through the posterior half of the pterygoid, ventrolateral to the braincase, though this canal bifurcates with medial branch exiting within the *sella turcica* on the dorsal surface of the *rostrum basisphenoidale* . This medial branch is not used by the internal carotid artery, but instead it is occupied by the cranial nerve (*Evers et al.* 2019B). The pterygoid has a large *crista pterygoidei which* contributes to the anterior wall of the braincase. This projection contacts and medially laps the epipterygoid. The epipterygoid is a small flat bone, contacting the parietal dorsally to form a laterally compressed vertical pillar anterior to the prootic. The contact between pterygoid and epipterygoid is barely visible in most specimens, and reportedly fuses

completely on occasion (Gaffney 1979). The *foramen nervi trigemini* is bounded by the prootic posteriorly and a pillar formed by the parietal, epipterygoid, and pterygoid anteriorly. (Fig 9).

Circumorbital series and temporal region

The orbital margin is composed of the maxilla, jugal, prefrontal, and postorbital (Fig 2). The frontal is consistently excluded from the orbit (Zangerl *et al.* 1988). Contrary to what is described in Limpus *et al.* (1988) the greatest width of the frontal occurs at the fronto-prefrontal suture, rather than the fronto-parietal suture (Fig. 3) (all three specimens). It is possible that this character varies between individuals, but a larger sample is required to estimate how variable.

The jugal of *N. depressus* is large compared to that of other extant sea turtle species, with the jugal almost equal in size to the postorbital bone or orbital opening (Fig. 2). The jugal of *N. depressus* significantly overlaps the quadratojugal: in places the contact is equal to a third of the length of the jugal; There is a prominent ridge which runs dorsoventrally through the posterior half of the jugal and on to the squamosal, quadratojugal and quadrate, Posterior to the ridge the bone is smooth and depressed compared to the rest of the external surface, while anterior to the ridge the surface is rougher and typical of the dorsal surface of the skull. (Fig. 2). The ridge and the differentiated regions do not correspond with the sutures of the head scalation (Fry 1913). The details of the associated soft anatomy were not resolvable in our scans. The anterior end of the jugal extends anteromedially alongside the palatal shelf of the maxilla and contacts the pterygoid and the palatine (Fig. 4).

In lateral view the exposed area of the quadratojugal is smaller compared to that of other sea turtles, largely due to the extensive overlap of the jugal. The external suture of the contact with the jugal is sigmoid, with a prominent anterior bow. The quadrate has a concave lateral surface which forms the medial surface of the *cavum tympani* (Fig. 2). The stapes passes through though the posterovenrally open *insisura columella auris* and the posteroventral margin of the quadrate. The ventral surface of the quadrate bears the mandibular condyle which comprises two smooth and shallow lobes. The lateral lobe

projects almost directly ventrally, whereas the medial lobe faces slightly medially. The condyle is anteroposteriorly short and in ventral aspect the two lobes are clearly separated, superficially resembling a figure eight (Fig. 4). The quadrate extends medially with the dorsal surface forming the floor of the posterior end of the adductor chamber. The quadrate encapsulates the lateral part of the *fenestra postoticus* (Fig. 2) (Ridgway *et al.* 1969). The channel that houses the stapes divides the bone into dorsal and ventral sections. The dorsal section of the medial surface contacts the opisthotic posteriorly and the prootic anteriorly. The ventral section contacts the pterygoid along its entire length. The anteromedial portion of the quadrate meets the lateral face of the prootic in a large and distinct boss to form the trochlear process.

Skull Roof

The skull roof is dominated by the large paired parietals, as well as including paired prefrontals, frontals, postorbitals, and squamosals (Fig. 3). The parietals are broad and relatively flat sloping away from where they meet in the midline. Each parietal contacts the postorbital and squamosal laterally, the frontal anteriorly, and the supraoccipital posteroventrally. The parietal has a large triangular projection on the ventral surface anteriorly: the *processus inferior parietalis*. This projection contributes to the lateral wall of the braincase and contacts the prootic and epipterygoid.

The squamosal contacts the quadrate, quadratojugal, postorbital, and parietal. The squamosal forms part of the lateral wall and the posterior wall of the adductor chamber. The extent of contact might reflect ontogeny given that the squamosal contacts the parietal late in development (Sheil 2013). The squamosal contacts the quadrate ventrally. The contact between the two is complex and extensive and migrates from the lateral wall of the skull medially across the floor of the adductor chamber. The entirety of the contact on the lateral wall occurs within the *cavum tympani*. There is an overhanging lip above this contact which forms the margin of the *cavum tympani* (Fig. 3). The posterior edge forms a significant portion of the margin of the *fossa temporalis superior*. The squamosal bears a single pronounced channel on its posterolateral corner, which serves as the site of origin for the musculus depressor mandibulae.

The postorbital forms most of the posterior margin of the orbit. Ventrally a thin spur-like structure extends between the orbit and the jugal, excluding the jugal from the orbit until the posteroventral corner. Anteriorly the postorbital contacts the prefrontal, excluding the frontal from the orbit. The dorsal margin is significantly longer than the ventral one.

Braincase

The braincase is a complex structure comprising the supraoccipital, exoccipitals, parietals, basioccipital, basisphenoid, opisthotic, prootic, parietal, epipterygoid, and pterygoid. The *condylus occipitalis* is concave bounded by three lobes: one ventral and two ventrolateral, with a dimple in the centre (Fig. 5). The basioccipital contributes the ventral lobe whereas the exoccipitals contribute the two ventrolateral lobes. The posterior face of the each of the paired exoccipitals is tall and tapers dorsomedially to contact the supraoccipital (Fig. 5). Medially the exoccipitals bound the *foramen magnum* which is roughly diamond-shaped (Fig. 5). The exoccipitals continue anteriorly and provide the posterolateral walls of the brain case. They contact the opisthotic posteriorly as well as laterally. They extend ventrally below the *condylus occipitalis* continuously in contact with the basioccipital, and form part of the dorsal margin of the opening of the *foramen posterior canalis cartotici interni*. The medial face makes up the posterolateral wall of the braincase and is perforated by two *foramina hypoglossi.* They continue to exit the exoccipital on the posterior face, on the posterolateral base of the occipital condyle. The posterior *foramen hypoglossi* is larger than the anterior one. *In N. depressus* there is a distinct *foramen jugulare posterius* consistently present in adult specimens (Fig 12). This feature is only found in *N. depressus* among Chelonioidea.

The opisthotic forms part of the lateral wall of the braincase. It contacts the squamosal laterally, the supraoccipital dorsally, and the prootic anteriorly (Fig 9). The anterior portion of the opisthotic houses much of the semicircular canals which is otherwise housed within the supraoccipital and prootic. The lateral face of the opisthotic contributes to the medial wall of the adductor chamber as well as the posterior shelf or floor. In medial view, the contribution of the opisthotic to the braincase appears to be fairly minimal, comprising a *processus interfenestralis* located between the *foramen jugulare anterius*

(posteriorly) and *hiatus acusticus* (anteriorly) (Fig. 9). The supraoccipital forms the dorsal margin of these two openings. In our specimens the *foramen jugulare anterius* is relatively large but is likely highly individually variable. In *N. depressus* there is a short triangular process of bone (from the opisthotic) protruding posteriorly along the anterior margin making the foramen more kidney-shaped than oval. In the Carettini and *E. imbricata* the foramen is narrow and crescent-like. The anterior edge of the medial face of the opisthotic forms the posterior margin of the *hiatus acusticus s* (Fig. 9). The *hiatus acusticus* itself is an irregular shape, having three distinct embayments (or lobes) extending posterodorsally, anterodorsally and ventrally. This shape is seen throughout Cheloniidae except for *Ch. mydas* where the *hiatus acusticus* is relatively narrower and the two dorsal most embayments are not as prominent. In *N. depressus*, the *posterior canalis semicularis* runs through the anterior portion of the opisthotic whereas the *anterior* and *lateral canalis semicularis*, run through much of the posteromedial portion of the prootic. The dorsal margin bears a small notch and is mainly formed by the prootic, the anterodorsal and anterior margins are also formed by the prootic, and the ventral margin is formed by the basisphenoid (Fig. 9).

The prootic is irregularly shaped and contacts the quadrate, pterygoid, basisphenoid, supraoccipital, opisthotic, and parietal. The prootic contributes to the medial wall of the braincase as well as the medial wall and floor of the adductor chamber (Fig. 9). The anterior margin forms most of the posterior edge of the *foramen trigemini.* Near the most dorsal point of this margin a small process extending into the foramen which is not found in the other species of sea turtle. The medial face forms a significant part of the braincase. The prootic is perforated on its medial face by the *fossa acustico-facialis,* which is roughly oval in shape. The *fossa acustico-facialis* contains three foramina, the most anterior foramen is the *foramen nervi facialis* which travels through the prootic to exit on the ventrolateral face, posterior to the *foramen trigemini.* The two posterior foramina are the *foramina nervi-acustici* (Fig. 10). The more medially located foramen perforates the posterior wall of the fossa into the inner ear. In *N. depressus* this foramen is fully enclosed, as is it is in most species.

The most conspicuous part of the supraoccipital is the *crista supraoccipitalis*. It is tongue-shaped in in lateral view and mediolaterally compressed forming a vertical blade of bone projecting posteriorly from the cranium (Fig. 2, 9). The lateral face is flat with a dorsal edge that is somewhat thicker than the rest of the projection. The anterior portion of the supraoccipital broadens considerably and forms most of the roof of the braincase. The ventral surface is concave structure and the ventral margins contact the exoccipital, opisthotic, and prootic.

The floor of the braincase is formed by the basioccipital posteriorly and the basisphenoid anteriorly. The basisphenoid contacts the basioccipital posteriorly, the external seam is relatively straight and oblique to the midline of the skull (Fig. 4). At the medial most point of contact to the basisphenoid, there is a small dorsally projecting tubercle on the basioccipital, the *basis tuberculi basalis*. This prominence is where the tendon of the Musculus retrahens Capiti Collique Pars Carapacobasioccipitalis muscle inserts (Jones *et al*. 2012). There is a low ridge of bone extending posteriorly from the *basis tuberculi basalis* along the midline of the basioccipital, and another running anteriorly along the midline of the basisphenoid. The basisphenoid has an anterior projection of bone the *rostrum basishphenoidale* (Fig. 11) which lies on the dorsal surface of the paired pterygoids along their midline contact. The dorsal surface of the basisphenoid is concave, and has two fairly large processes projecting anterodorsally just posterior to the *rostrum basisphenoidale*. This rostrum is relatively robust and squat in *N. depressus*, but, species in the Carettini have a thinner, longer rostrum. The basisphenoid has a ventrally projecting V-shaped crest, the tip of which merges with the central ridge along the medial contact between the two pterygoid bones. The contact is overlapping with the basisphenoid largely resting atop the pterygoids, the crest representing the posterior most contact.

Lower jaw

The lower jaw is V shaped in dorsal view, and relatively heavily built (Fig. 6, 7). The two dentaries are fused with no clear suture seam visible even in cross section (Fig. 6). The tip of the dentary is located dorsal to the long-axis of the Mecklian groove (Fig. 6). The labial and lingual ridges of *N. depressus* are prominent and both form a distinct midline point; there is a distinct ridge connecting these

two points. The point of the lingual margin is almost as large as the point on the labial ridge; it is visible in lateral view, there is a distinct ridge connecting the two peaks of the lingual and labial margin. There is a large triangular depression on the lateral surface of the dentary. It deepens anteriorly eventually leading to the *foramen dentofaciale majus*, this travels anteriorly through the dentary meeting its counterpart at the midline of the mandibular symphysis (Fig. 6). From the *foramen dentofaciale majus* to the articular surface runs a distinct shelf along the ventral portion of the lateral surface of the lower jaw (Fig. 6). This shelf is formed at its most posterior portion by the dentary, but the majority of it is formed by the suran gular. This shelf is likely related to the insertion point of the M. adductor mandibulae externus Pars superficialis (Jones *et al*. 2012). The medial face of the dentary is marked by a very obvious Meckelian groove. It runs the entire length of the dentary at mid-depth. The dentary has a large posterolateral process. The dentary contacts the surangular posterolaterally, the surangular dorsally, and the coronoid posterodorsally and medially, as well as the angular posteriorly and posteromedially (Fig. 6).

The surangular is a largely flat sheet of bone making up most of the posterior half of the lateral face of the lower jaw (Fig. 6). Anterodorsally it contacts the coronoid there is also posterior and posterodorsal contact with the articular, and ventral contact with the dentary and angular. Posteriorly it has anteromedially curved processes that contact the prearticular. The *fossa Meckelii* is bound laterally by the surangular, anteriorly by the coronoid, medially by the prearticular, and posteriorly by the articular. The *fossa Mekellii* continues to the medial face. The articular surface at its posterior extremity on the lower jaw mirrors the surface of the condyle of the quadrate (Fig. 6, 7) (although in life both surfaces would be capped with cartilage, e.g. Jones *et al*. 2012). The lower end of the external suture seam between the dentary and surangular passes anteriorly before it passes posteroventrally (e.g. WAM R112123) in contrast to the simpler posteroventral path figured by Hirayama (1994: Fig. 5).

The biting surface is comprised of two shallow troughs either side of a subtle parasagittal ridge. The medial trough has anterior and posterior concavities and is formed by the dorsal face of the articular. The lateral trough is formed by the surangular. At the anterior most point there is a transverse ridge. A less prominent ridge also protrudes at the posterior end of the articular surface (where the articular and

surangular meet posteriorly). At least in these specimens, the contact between the surangular and articular is difficult to see, unlike other species where the seam is clear. This might be due to specimen preparation or other post mortem effects. The articulating surface faces posterodorsally. The angular lies along the ventromedial edge of the lower jaw. It contributes to the most posterior section of the Mekelian groove (Fig. 6). The prearticular is a large flat bone constituting much of the posterior section of the medial face. Though largely flat it does curve medially near the articular surface. From medial view the prearticular contacts the coronoid anteriorly. The coronoid sits atop the surangular, dentary, and prearticular.

PHYLOGENETIC RELATIONSHIPS

All four datasets found generally the same topology, but with key differences for Chelonioidea and closely related taxa (Fig. 13 - 14).

The results from all datasets place, *Toxochelys spp.* as the sister taxon to the rest of Pan-Chelonioidea and Protostegidae is a distinct sister clade to a clade including Cheloniidae and Dermochelyidae as is found in recent studies (Evers 2019; Gentry *et al.* 2019). It should be noted that the polytomy at the base of the tree is likely an artefact of character selection to optimise resolving relationships within Pan-Chelonioidea and does not reflect the relative phylogenetic position of these two genera.

Results from data set A (Includes the 23 taxa of interest and only the characters used in Evers and Benson 2019) (Fig. 13) recovers Chelonioidea (P = 0.99). Crown cheloniids form a monophyletic group (P = 0.83). Dermochelyidae (*Dermochelys coriacea* + *Eosphargis breineri*) is recovered with strong support (P= 1). A clade comprising three American fossil taxa (*Carolinachelys winsonii, Procolpochelys grandavea, + Pacifichelys hutchisoni*) is well supported (P= 0.93) and is sister to *Allopleuron hoffmani* though with weak support (P = 0.28). *Argillochelys cuneiceps* and *Puppigerius camperi* are along the stem of Cheloniidae, though their placement there has weak support. *Chelonia mydas* and *N. depressus* do not form a clade and instead *N. depressus* falls as sister to the rest of the crown, with *Ch. mydas* as sister to the *E. imbricata* + Carettini clade.

Results from dataset C (includes all of the taxa and only the characters used in Evers and Benson (2019)) recovered Pan-Chelonioidea (P =1) (Fig 14). However, Cheloniidae was not recovered, with Dermochelyidae nested within Cheloniid turtles as a sister to *Ch. mydas* (P = 0.74). *Natator depressus* was recovered as sister to the rest of the crown and the *Ch. mydas* + Dermochelyidae group (P= 0.81).

Results from data set B (includes the taxa of interest and the new characters found in this study) recovers Chelonioidea and it is well supported (P=0.99) (Fig. 13). Crown cheloniids form a monophyletic group with high support (P = 0.95), and with a branching order identical to the consensus hypothesis based on analysis of molecular data (e.g. Naro-Maciel *et al.* 2008; Duchene *et al.* 2012). That is, *N. depressus* is placed in a clade with *Ch. mydas*, and this pair is sister to the remaining cheloniids, with *E. imbricata* the sister of the Carettini. Dermochelyidae are sister to Cheloniidae. *Eochelone brabantica* is sister to the rest of Cheloniidae (P = 0.82). The clade of American cheloniids (P =0.94) (*Carolinachelys wilsonii, Procolpochelys grandavea, + Pacifichelys hutchisoni*) is again recovered, as well as the sister relationship to *Allopleuron hoffmani* (P = 0.26). The topology for crown group Cheloniidae recovered matches that recovered with molecular evidence, and *N. depressus* is recovered as sister to *Ch. mydas* (P = 0.62).

Results from dataset D (s includes the all the taxa from Evers *et al.* 2019 and the new characters) are largely consistent with the trees recovered using dataset B (Fig 14). The support values are generally weaker, likely due to the necessity of marking the new characters as unknown in many taxa. The topology of the crown group recovered is consistent with the current molecular consensus (Naro-Maciel *et al* 2008; Duchene *et al* 2012).

DISCUSSION

Natator depressus exhibits several skull features which have not been reported previously. These features include a proportionately large jugal with a high degree of overlap with the quadratojugal, the well-defined superficial jugal ridge as well as the fully enclosed *foramen jugulare posterius*. The function of

these features is unclear. The extensive jugal overlap might relate to the size or shape of the *adductor mandibulae externus pars superficialis,* which has one of three origin points contacting the anterior of the quadratojugal and posterior of the jugal (Jones *et al.* 2012). The greater overlap provides greater surface area for associated connective tissues and therefore might reflect the temporal region being subjected to relatively greater strain than in other sea turtles (Jaslow 1990; Jones *et al*. 2011). The functionality of the superficial jugal ridge is unclear. Though there is evidence of this feature in all species of sea turtles it is particularly prominent in *N. depressus* It is possible that this structure is associated with the middle ear. The prominent ridge in *N. depressus* is associated with a relatively large jugal but why the ridge is so prominent is unclear. There has been little work focusing on the external surface of the ear region of sea turtles, summarised in Bartol and Musick (2003). The prominence of the ridge may be related to the attachment of the disk of subcutaneous fat underlying the scales of the ear region (Henson 1974; Ridgway *et al.* 1969, Bartol and Musick 2003). The attachment of the cutaneous plate on the exterior of the ear of *Ch. mydas* is reported to be loose (Ridgway *et al.* 1969); perhaps the attachment is firmer in *N. depressus*. A slightly different arrangement of the of this structure in *N. depressus* would be interesting given that it is a shallow water specialist, and the only modern sea turtle without a pelagic life stage (Limpus *et al.* 1983; Walker and Parmenter 1990). The auditory ability of Testudines has recently received some attention (e.g. Christensen-Dalsgaard *et al.* 2012; Piniak *et al.* 2012; Willis 2016), but the functional anatomy of the ear is generally considered to be poorly known. A recent study by Foth *et al.* (2019) was unable to identify a relationship between middle ear shape and habitat ecology in turtles.

As stated in previous studies (Zangerl *et al* 1988; Limpus *et al* 1988), the general shape of the skull of *N. depressus* resembles *L. olivacea*: relatively wide skull, a broad palate, large external pterygoid processes. Several other features shared by the two species such as the shape of the *hiatus acousticus,* the orientation of the origin of the *depressor mandibulae,* and the size and location of foramina are shared by multiple species. The size of the *crista supraoccipitalis* is notably smaller than it is in other species, but it is perhaps most similar to *E. imbricata.* The shape of the *crista supraoccipitalis* is broad and rounded in contrast to *Ch. mydas* in which it is pointed and narrow. Like *Ch. mydas* but unlike other extant members

of Chelonioidea, the maxilla has a significant portion lying ventral to the jugal in lateral view, a squared posterior edge, and ventral ridges.

Overall the lower jaw of *Natator depressus* resembles that of *Chelonia mydas.* It has a distinct sharp lingual and labial ridge on the dentary, with distinct anterior peaks connected by a distinct midline ridge. It lacks the large flattened area at the anterior of the dentaries found in members of Carettini. The coronoid process is significantly smaller than that of *L. olivacea* and *Ca. caretta.* Unlike both *E. imbricata* and *Ch. mydas* there is no ventral flexion at the anterior tip. There is a large variation in the direction of the mandibular articulation within crown Cheloniidae. In *N. depressus* the articulating surface faces postero-dorsally, in *Ch. mydas* the surface faces more dorsally whereas in *Ca. caretta* it faces almost entirely posteriorly. Characters previously used to unite *N. depressus* and *Lepidochelys* spp. appear to vary within the two species or appear to be plesiomorphic for the crown of Cheloniidae (Limpus *et al.* 1988; Zangerl *et al.* 1988). Unlike what is suggested in Limpus *et al.* (1988) the contact of the prefrontal and postorbital does not occur in our sample of *L. olivacea* suggesting that it might be a variable character trait within this species (Pritchard and Trebbau 1984; Zangerl *et al* 1988, Wyneken and Witherington 2001; Jones *et al*. 2012; SAMA BM670; SMNS 11070).

In this study it was found that *Natator depressus* and *Chelonia mydas* share the following synapomorphies, a robust *rostrum basisphenoidale* and a squared off maxillary margin. Some of the other distinguishing features of *N. depressus* reported in this study, the distinct superficial jugal ridge and the extensive overlap of the quadratojugal by the jugal, are present to a lesser extent in *Ch. mydas*. The two species also completely lack a posterolateral jugal process, unlike all other species within crown Cheloniidae.

Although our study finds a number of character traits shared by *Chelonia mydas* and *Natator depressus*, the two species also show some marked differences. *Ch. mydas* has a notably blunt snout compared to other species as well as a posteriorly directed origin for the depressor mandibulae. The rectangular shape of the *hiatus acusticus* in *Ch. mydas* is markedly different from the other species (Fig. 10). Some of the difference in general skull shape could potentially be explained by the anteroposteriorly

short rostrum and herbivorous diet of *Ch. mydas* (Bjorndal *et al.* 1997). The cranial similarities presented in Limpus *et al.* (1988) previously considered to indicate a close affinity between *N. depressus* and *L. olivacea,* instead highlight the strangeness of *Ch. mydas*. These data as well as our new observations suggest that *Ch. mydas* is not a particularly appropriate representative taxon for Cheloniidae.

This revision of *Natator depressus* provides another example of a study that has uncovered morphological evidence for a phylogenetic hypothesis that was previously considered supported mainly by molecular data (e.g. Asher and Geisler 2008; Lee and Camens 2009). Molecular frameworks can be valuable for analysing the datasets that include fossil taxa. However, a more comprehensive examination of modern species, particularly skeletal characters, is needed so that their morphological traits can be included within phylogenetic analyses (e.g. Nick 1912; Bell and Mead 2014, Regnault et al. 2017). In most cases, skeletal characters are the only means of direct comparison between fossil taxa and extant taxa. Such practice will increase our understanding of character distribution, character polarity and character evolution in the crown group. This achievement is necessary to correctly distinguishing between crown vs stem taxa in the fossil record. Coupled with tip and node dating methods (e.g. Lourenco et al. 2012; Lee and Yates 2018), it may be possible to resolve the total group phylogenetic relationships and address broader macroevolutionary questions.

CONCLUSION

This study recovers a sister group relationship between *Natator depressus* and *Chelonia mydas* using a quantitative analysis of only morphological evidence. This is, to the best of our knowledge, the first time the currently accepted phylogenetic tree has been found using quantitative methods without a molecular constraint. The synapomorphies uniting *N. depressus* and *Ch. mydas* found in this study: overlap of the quadratojugal by the jugal, a superficial ridge transecting the jugal, a squared off maxillary margin, and a robust *rostrum basisphenoidale.* The characters shared by *N. depressus* and *Lepidochelys* spp. are also shared with other cheloniids. It is notable that the braincase features that appear to unite *N. depressus* and

Ch. mydas were not examined by previous studies This apparent omission likely relates to the previous difficulty of evaluating such characters without destructive sampling and highlights the potential unlocked by greater availability of micro Computed Tomographic imaging. The new characters identified here should be included in future studies of fossil sea turtles and CT scanning may help make this task possible.

LITERATURE CITED

Abreu-Grobois A, Plotkin P, (IUCN SSC Marine Turtle Specialist Group). 2008. *Lepidochelys olivacea*. *The IUCN Red List of Threatened Species* **2008:** 6–8.

Asher RJ, Geisler JH, Sánchez-Villagra MR. 2008. Morphology, paleontology, and placental mammal phylogeny. *Systematic Biology* **57:** 311–317.

Asher RJ, Lehmann T. 2008. Dental eruption in afrotherian mammals. *BMC Biology* **6(14):** 1–11.

Bardet N, Jalil NE, de Lapparent de Broin F, Germain D, Lambert O, Amaghzaz M. 2013. A giant chelonioid turtle from the Late Cretaceous of Morocco with a suction feeding apparatus unique among tetrapods. *PLoS ONE* **8:** e63586.

Bartol SM, Musick JA. 2003. Sensory biology of sea turtles. *The biology of sea turtles* **2:** 79–102.

Baur G. 1890. The genera of the Cheloniidae. *American Naturalist* **1890:** 486–487.

Benton MJ. 2008. Classification and phylogeny of the diapsid reptiles. *Zoological Journal of the Linnean Society* **84:** 97–164.

Bjorndal KA. 1985. Nutritional ecology of sea turtles. *Copeia* **1985:** 736–751.

Bjorndal KA, Lutz P, Musick J. 1997. Foraging ecology and nutrition of sea turtles. *The biology of sea turtles* **1:** 199–231.

Bowen BW, Nelson WS, Avise JC. 1993. A molecular phylogeny for marine turtles: trait mapping, rate assessment, and conservation relevance. *Proceedings of the National Academy of Sciences* **90:** 5574–5577.

Brinkman D, Aquillon-Martinez MC, de Leon Dávila C, Jamniczky H, Eberth DA, Colbert M. 2009. *Euclastes coahuilaensis* sp. nov., a basal cheloniid turtle from the late Campanian Cerro del Pueblo Formation of Coahuila State, Mexico. *PaleoBios* **28:** 76–88.

Buskirk JV, Crowder LB. 1994. Life-history variation in marine turtles. *Copeia* **1994:** 66–81.

Cadena EA, Parham JF. 2015. Oldest known marine turtle? A new protostegid from the Lower Cretaceous of Colombia. *PaleoBios* **32:** 1–42.

Cardini A, Elton S. 2008. Does the skull carry a phylogenetic signal? evolution and modularity in the guenons. *Biological Journal of the Linnean Society* **93:** 813–834.

Casale P, Tucker AD. 2017. *Caretta caretta* (amended version of 2015 assessment). *The IUCN Red List of Threatened Species* **2017.** http://dx.doi.org/10.2305/IUCN.UK.2017-2.RLTS.T3897A119333622.en. Date accessed: 29 November 2019.

Christensen-Dalsgaard J, Brandt C, Willis KL, Christensen CB, Ketten D, Edds-Walton P, Fay RR, Madsen PT, Carr CE. 2012. Specialization for underwater hearing by the tympanic middle ear of the turtle, *Trachemys scripta* elegans. *Proceedings of the Royal Society B: Biological Sciences* **279:** 2816–2824.

Cordero GA, Quinteros K, Janzen, FJ. 2018. Delayed trait development and the convergent evolution of shell kinesis in turtles. *Proceedings of the Royal Society B*, **285(1888):** p 20181585.

Crawford NG, Parham JF, Sellas AB, Faircloth BC, Glenn TC, Papenfuss TJ, Henderson JB, Hansen MH, Simison WB. 2015. A phylogenomic analysis of turtles. *Molecular Phylogenetics and Evolution* **83:** 250–257.

Dodd CKJ. 1988. Synopsis of the biological data on the loggerhead sea turtle *Caretta caretta* Linnaeus 1758. *U S Fish and Wildlife Service Biological Report* **88:** 1–110.

Donoghue MJ, Doyle JA, Gauthier J, Kluge AG, Rowe T. 1989. The importance of fossils in phylogeny reconstruction. *Annual review of Ecology and Systematics* **20:** 431–460.

Duchene S, Frey A, Alfaro-Nunez A, Dutton PH, Gilbert MTP, Morin PA. 2012. Marine turtle mitogenome phylogenetics and evolution. *Molecular Phylogenetics and Evolution* **65:** 241–250.

Dutton PH, Davis SK, Guerra T, Owens D. 1996. Molecular phylogeny for marine turtles based on sequences of the ND4-leucine tRNA and control regions of mitochondrial DNA. *Molecular Phylogenetics and Evolution* **5:** 511–521.

Emerson SB, Bramble DM. 1993. Scaling, allometry, and skull design. *The skull* **3:** 384-421.

Eschscholtz JF. 1829. *Zoologischer Atlas, enthaltend Abbildungen un Beschreibungen neur Thierarten, während des Flottcapitains von Kotzebue zweiter Reise um die Welt. 1823-1826 beobacht.* Reimer.

Evers SW, Benson RBJ. 2019. A new phylogenetic hypothesis of turtles with implications for the timing and number of evolutionary transitions to marine lifestyles in the group. *Palaeontology* **62:** 93–134

Evers SW, Barrett PM, Benson, RBJ. 2019. Anatomy of Rhinochelys pulchriceps (Protostegidae) and marine adaptation during the early evolution of chelonioids. *PeerJ* **7:** e6811.

Evers SW, Neenan JM, Ferreira GS, Werneburg I, Barrett PM, Benson RBJ. (2019)B. Neurovascular anatomy of the protostegid turtle Rhinochelys pulchriceps and comparisons of membranous and endosseous labyrinth shape in an extant turtle. *Zoological Journal of the Linnean Society* **187:** 800–828.

Ferreira GS, Rincón AD, Solórzano A, Langer MC. 2015. The last marine pelomedusoids (Testudines: Pleurodira): a new species of Bairdemys and the paleoecology of Stereogenyina. *PeerJ* **3:** e1063.

Foth C, Evers SW, Joyce WG, Volpato VS, Benson RBJ (2019) Comparative analysis of the shape and size of the middle ear cavity of turtles reveals no correlation with habitat ecology. *Journal of Anatomy* **235:** 1078–1097.

Frazier J. 1985. Misidentifications of Sea Turtles in the East Pacific: *Caretta caretta* and *Lepidochelys olivacea*. *Journal of Herpetology* **19:** 1–11.

Fry DB. 1913. On the status of *Chelonia depressa* Garman. *Records of the Australian Museum* **10:** 159–185.

Gaffney ES. 1972. An illustrated glossary of turtle skull nomenclature. *American Museum Novitates* **2486:** 1–33.

Gaffney ES. 1979. Comparative cranial morphology of recent and fossil turtles. *Bulletin of the American Museum of Natural History* **164:** 65–376.

Gaffney ES, Meylan P. 1988. A phylogeny of turtles. In: Benton MJ ed. *The phylogeny and classification of the tetrapods. Volume 1: Amphibians, Reptiles, Birds*. Oxford: Clarendon Press, 157–219.

Garman S. 1880. On certain species of Chelonioidae. *Bulletin of the Museum of Comparative Zoology at Harvard College* **6:** 123–126.

Gatesy J, Amato G, Norell M, DeSalle R, Hayashi C. 2003. Combined Support for Wholesale Taxic Atavism in Gavialine Crocodylians. *Systematic Biology* **52:** 403–422.

Geisler JH, Uhen MD. 2003. Morphological support for a close relationship between hippos and whales. *Journal of Vertebrate Paleontology* **23:** 991–996.

Gentry, AD. (2017). New material of the Late Cretaceous marine turtle Ctenochelys acris Zangerl, 1953 and a phylogenetic reassessment of the 'toxochelyid'-grade taxa. *Journal of Systematic Palaeontology* **15:** 675–696.

Gentry AD, Ebersole JA, Kiernan CR. 2019. *Asmodochelys parhami*, a new fossil marine turtle from the Campanian Demopolis Chalk and the stratigraphic congruence of competing marine turtle phylogenies. *Royal Society Open Science* **6:** 191950.

Hanken J, Thorogood P. 1993. Evolution and development of the vertebrate skull: The role of pattern formation. *Trends in Ecology & Evolution* **8:** 9–15.

Hasegawa Y, Hirayama R, Kimura T, Takakuwa Y, Nakajima H, Club GF. 2005. Skeletal restoration of fossil sea turtle, Syllomus, from the Middle Miocene Tomioka Group, Gunma Prefecture, Central Japan. *Bulletin of the Gunma Museum of Natural History* **9:** 29–64.

Hirayama R 1994. Phylogenetic systematics of chelonioid sea turtles. *Island Arc* **3:** 270–284.

Henson OW. (1974). Comparative Anatomy of the Middle Ear. In 'Auditory System: Anatomy Physiology (Ear).' (Eds WD Keidel, WD Neff.) pp. 39–110. (Springer Berlin Heidelberg: Berlin, Heidelberg)

Hirayama R. 1998. Oldest known sea turtle. *Nature* **392:** 705–708.

Jaslow CR. 1990. Mechanical properties of cranial sutures. *Journal of Biomechanics* **23:** 313–321.

Jones MEH, Curtis N, Fagan MJ, O'Higgins P, Evans SE. 2011. Hard tissue anatomy of the cranial joints in *Sphenodon* (Rhynchocephalia): sutures, kinesis, and skull mechanics. *Palaeontologia Electronica* **14(2), p.17A:** 1–92.

Jones MEH, Werneburg I, Curtis N, Penrose R, O'Higgins P, Fagan MJ, Evans SE. 2012. The head and neck anatomy of sea turtles (Cryptodira: Chelonioidea) and skull shape in testudines. *PLoS ONE* **7:** e47852.

Kear BP, Lee MSY. 2006. A primitive protostegid from Australia and early sea turtle evolution. *Biology Letters* **2:** 116–119.

Kesteven HL. 1911. The anatomy of the head of the green turtle, *Chelone midas* Latr. Part 1. The skull. *Proceedings of the Royal Society of New South Wales* **44:** 368–400.

Lee MSY. 2001. Molecules, morphology, and the monophyly of diapsid reptiles. **70**. 1.

Lee MSY. 2013. Turtle origins: insights from phylogenetic retrofitting and molecular scaffolds. *Journal of Evolutionary Biology* **26:** 2729–2738.

Lee MSY, Yates AM. 2018. Tip-dating and homoplasy: reconciling the shallow molecular divergences of modern gharials with their long fossil record. *Proceedings of the Royal Society B: Biological Sciences* **285:** 20181071.

Legg DA, Sutton MD, Edgecombe GD. 2013. Arthropod fossil data increase congruence of morphological and molecular phylogenies. *Nature Communications* **4:** 2485.

Lewis PO. 2001. A Likelihood Approach to Estimating Phylogeny from Discrete Morphological Character Data. *Systematic Biology* **50:** 913–925.

Limpus C. 2007. A biological review of Australian marine turtles. 5. Flatback turtle, *Natator depressus* (Garman). Brisbane, Queensland: Queensland Environmental Protection Agency.

Limpus C, Parmenter, C, Baker V, Fleay A. 1983. The flatback turtle, *Chelonia depressa*, in Queensland: Post-Nesting migration and feeling ground distribution. *Wildlife Research* **10:** 557–561.

Limpus CJ, Gyuris E, Miller JD. 1988. Reassessment of the taxonomic status of the sea turtle genus *Natator* McCulloch, 1908, with a redescription of the genus and species. *Transactions of The Royal Society of South Australia* **112:** 1–10.

Linnaeus C. 1758. *System Naturae, per Regna Tria Naturae, secundum Classes, Ordines, Genera, Species, cum Characteribus, Differemtiis, Synonymis, Locis, Tomus* I. Edito Decima, Reformata. [10th Ed.] Holimae [Stockholm]:Laurentii Salvi.

Linnaeus C. 1766. *Systema naturae*. Edito Duodecima. Reformata. Tomus I, Pars I, Regnum Animale. [12th Ed.]. Holmiae [Stockholm]: Laurentii Salvii.

Lourenco JM, Claude J, Galtier N, Chiari, Y. 2012. Dating cryptodiran nodes: origin and diversification of the turtle superfamily Testudinoidea. *Molecular Phylogenetics and Evolution* **62:** 496–507.

Lynch S, Parham J. 2003. The first report of hard-shelled sea turtles (Cheloniidae sensu lato) from the Miocene of California, including a new species (*Euclastes hutchisoni*) with unusually plesiomorphic characters. *PaleoBios* **23:** 21–35.

McInerney PL, Lee MSY, Clement AM, Worthy TH. 2019. The phylogenetic significance of the morphology of the syrinx, hyoid and larynx, of the southern cassowary, *Casuarius casuarius* (Aves, Palaeognathae). *BMC Evolutionary Biology* **19:** 233.

McCormack JE, Faircloth BC. 2013. Next-generation phylogenetics takes root. *Molecular Ecology* **22:** 19–21.

McCulloch AR. 1908. A new genus and species of turtle: from North Australia. *Records of the Australian Museum* **7:** 126–128.

Mortimer JA, Donnelly M. (IUCN SSC Marine Turtle Specialist Group) 2008. *Eretmochelys imbricata*. *The IUCN Red List of Threatened Species* **2008** http://dx.doi.org/10.2305/IUCN.UK.2008.RLTS.T8005A12881238.en. Date accessed 29 November 2019

Müller J, Reisz RR. 2005. Four well-constrained calibration points from the vertebrate fossil record for molecular clock estimates. *BioEssays* **27**: 1069–1075.

Müller J, Reisz RR, Lee M. 2006. The phylogeny of early eureptiles: comparing parsimony and Bayesian approaches in the investigation of a basal fossil clade. *Systematic Biology* **55:** 503–511.

Naro-Maciel E, Le M, FitzSimmons NN, Amato G. 2008. Evolutionary relationships of marine turtles: A molecular phylogeny based on nuclear and mitochondrial genes. *Molecular Phylogenetics and Evolution* **49:** 659–662.

Nielsen E. 1959. Eocene turtles from Denmark. *Bulletin of the Geological Society of Denmark* **14**: 96–114.

Nishizawa H, Asahara M, Kamezaki N, Arai N 2010. Differences in the skull morphology between juvenile and adult green turtles: implications for the ontogenetic diet shift. *Current Herpetology* **29:** 97–101.

Nylander JAA, Ronquist F, Huelsenbeck JP, Nieves-Aldrey J. 2004. Bayesian Phylogenetic Analysis of Combined Data. *Systematic Biology* **53:** 47–67.

Parham. JF, Fastovsky DE. 1997. The phylogeny of cheloniid sea turtles revisited. *Chelonian Conservation and Biology* **1:** 548–554.

Parham JF, Pyenson ND. 2010. New sea turtle from the Miocene of Peru and the iterative evolution of feeding ecomorphologies since the Cretaceous. *Journal of Paleontology* **84:** 231-247.

Piniak WED, Mann DA, Eckert SA, Harms CA. 2012. Amphibious hearing in sea turtles. In: Popper AN, Hawkins A ed. *The effects of noise on aquatic life*. New York, Springer New York, 83–87.

Pritchard PCH, Trebbau P. 1984. *The Turtles of Venezuela.* Oxford, Ohio: Society for the Study of Amphibians and Reptiles.

Pyron RA. 2011. Divergence Time Estimation Using Fossils as Terminal Taxa and the Origins of Lissamphibia. *Systematic Biology* **60:** 466–481.

Raselli I. 2018. Comparative cranial morphology of the Late Cretaceous protostegid sea turtle Desmatochelys lowii. *PeerJ* **6:** e5964.

Regnault S, Hutchinson JR, Jones ME. 2017. Sesamoid bones in tuatara (*Sphenodon punctatus*) investigated with X-ray microtomography, and implications for sesamoid evolution in Lepidosauria. *Journal of Morphology* **278:** 62–72.

Ridgway SH, Wever EG, McCormick JG, Palin J, Anderson JH. 1969. Hearing in the giant sea turtle, *Chelonia mydas*. *Proceedings of the National Academy of Sciences* **64:** 884–890.

Ronquist F, Teslenko M, van der Mark P, Ayres DL, Darling A, Höhna S, Larget B, Liu L, Suchard MA, Huelsenbeck JP. 2012. MrBayes 3.2: Efficient Bayesian Phylogenetic Inference and Model Choice Across a Large Model Space. *Systematic Biology* **61:** 539–542.

San Mauro D, Agorreta A. 2010. Molecular systematics: a synthesis of the common methods and the state of knowledge. *Cellular and Molecular Biology Letters* **15:** 311–341.

Schnitzler J, Theis C, Polly PD. Eronen JT. 2017. Fossils matter–understanding modes and rates of trait evolution in Musteloidea (Carnivora). *Evolutionary Ecology Research*, **18:** 187–200.

Seminoff JA. (Southwest Fisheries Science Center, U.S.) 2004. *Chelonia mydas*. *The IUCN Red List of Threatened Species* 2004: http://dx.doi.org/10.2305/IUCN.UK.2004.RLTS.T4615A11037468.en. Date accessed 29 November 2019

Shaffer HB, Meylan P, McKnight ML. 1997. Tests of turtle phylogeny: molecular, morphological, and paleontological approaches. *Systematic Biology* **46:** 235–268.

Sheil CA. 2013. Development of the skull of the hawksbill sea turtle, *Eretmochelys imbricata*. *Journal of Morphology* **274:** 1124–1142.

Surkov MV, Benton MJ. 2004. The basicranium of dicynodonts (Synapsida) and its use in phylogenetic analysis. *Palaeontology* **47(3):** 619-638.

Vandelli D. 1761. *Epistola de Holothurio, et Testudine Coriacea ad Celeberrimum Carlum Linnaeum*. Padova: Patavii Conzatti.

Walker TA, Parmenter CJ. 1990. Absence of a pelagic phase in the life cycle of the flatback turtle, *Natator depressa* (Garman). *Journal of Biogeography* **17:** 275–278.

Wallace BP, Tiwari M, Girondot M. 2013. *Dermochelys coriacea*. *The IUCN Red List of Threatened Species* 2013. http://dx.doi.org/10.2305/IUCN.UK.2013-2.RLTS.T6494A43526147.en. Date accessed 29 November 2019

Watanabe A, Slice DE. 2014. The utility of cranial ontogeny for phylogenetic inference: a case study in crocodylians using geometric morphometrics. *Journal of Evolutionary Biology* **27:** 1078–1092.

Weems RE. 1980. Syllomus aegyptiacus, a Miocene pseudodont sea turtle. *Copeia* **1980:** 621–625.

Weems RE, Sanders AE. 2014. Oligocene pancheloniid sea turtles from the vicinity of Charleston, South Carolina, USA. *Journal of Vertebrate Paleontology* **34:** 80–99.

Weems RE, Brown KM. 2017. More-complete remains of *Procolpochelys charlestonensis* (Oligocene, South Carolina), an occurrence of *Euclastes* (upper Eocene, South Carolina), and their bearing on Cenozoic pancheloniid sea turtle distribution and phylogeny. *Journal of Paleontology* **91:** 1228–1243.

Wibbels T, Bevan E. 2019. *Lepidochelys kempii*. *The IUCN Red List of Threatened Species* 2019: http://dx.doi.org/10.2305/IUCN.UK.2019-2.RLTS.T11533A142050590.en. Date accessed 29 November 2019

Wiens. JJ. 2009. Paleontology, Genomics, and Combined-Data Phylogenetics: Can Molecular Data Improve Phylogeny Estimation for Fossil Taxa? *Systematic Biology* **58:** 87–99.

Williams EE, Grandison AGC, Carr AF. 1967. *Chelonia depressa* Garman re-investigated. *Breviora* **271:** 1–15.

Willis KL. 2016. Underwater hearing in turtles. In: Popper A, Hawkins A eds. *The effects of noise on aquatic life II*. New York: Springer. **875:** 1229–1235.

Wyneken J. 2001. The anatomy of sea turtles. *U.S. Department of Commerce NOAA Technical Memorandum* **NMFS-SEFSC-470:** 1–172.

Zangerl R. 1980. Patterns of Phylogenetic Differentiation in the Toxochelyid and Cheloniid Sea Turtles. *American Zoologist* **20:** 585–596.

Zangerl R, Hendrickson LP, Hendrickson JR. 1988. A redescription of the Australian flatback sea turtle, *Natator depressus*. *Bishop Museum Bulletin of Zoology* **1:** 1–69

Table 1. State of characters found in this study detailed further in Appendix 1

New Character	***N. depressus***	***Ch. mydas***	***E. imbricata***	***Ca. caretta***	***L. olivacea***	***L. kempii***
Anterior foramen hypoglossi *alignment compared to that of the midline of the* acoustic facialis	Ventral	In line	Ventral	Ventral	Ventral	Ventral
Relative *size of the two posterior foamina of the* nervi hypoglossi	Variable	Anterior foramen less than half of the diameter of posterior foramen	Anterior foramen less than half of the diameter of the posterior foramen	Similar in size	Similar in size	Similar in size
*Anterior process intruding into the f*oramen trigemini	Process present	Process absent	Process absent	Process absent	Process absent	Process absent
The shape of the rostrum basisphenoidale	Robust, with large processes	Robust, with large processes	gracile with small processes	gracile with small processes	gracile with small processes	gracile with small processes
The shape of the labial margin of the maxilla	Labial margin of maxilla squared off	Labial margin of maxilla squared off	Labial margin of maxilla continuous with jugal	Labial margin of maxilla continuous with jugal	Labial margin of maxilla continuous with jugal	Labial margin of maxilla continuous with jugal
The extent of the superficial ridge on the jugal	Distinct superficial ridge transecting jugal	Indistinct margin transecting jugal	No ridge along the jugal	No ridge along the jugal	No ridge along the jugal	No ridge along the jugal
The shape of the hiatus acousticus	Hiatus acousticus has two distinct sections with the dorsal portion significantly wider than the ventral portion	Hiatus acousticus is largely rectangular with no significant difference in width between the dorsal and ventral portions	Hiatus acousticus has two distinct sections with the dorsal portion significantly wider than the ventral portion	Hiatus acousticus has two distinct sections with the dorsal portion significantly wider than the ventral portion	Hiatus acousticus has two distinct sections with the dorsal portion significantly wider than the ventral portion	Hiatus acousticus has two distinct sections with the dorsal portion significantly wider than the ventral portion
The presence of a posteroventrally extenging process from the jugal	No process	No process	Small process	Small process	Large process extending posterior to the jugal-quadratojugal margin	Large process extending posterior to the jugal-quadratojugal margin
Degree of overlap of the jugal on the quadratogual	Extensive overlap	Marginal overlap	Negligible overlap	Negligible overlap	Negligible overlap	Negligible overlap
Orientation of the surface which provides the origin of the depressor mandibulae	Faces laterally or posterolaterally	Faces posteriorly	Faces laterally or posterolaterally	Faces laterally or posterolaterally	Faces laterally or posterolaterally	Faces laterally or posterolaterally

from the squamosal						

APPENDIX 1

The new characters found in this study for *Natator* and the other sea turtles mainly involve features of the braincase and temporal region:

1. Anterior foramen *nervi hypoglossi* posterior opening when ventral surface of braincase is horizontal: ventral to *acustico facialis* (0); in line with *acustico facialis* (1) Fig. 9.
2. Size of the two posterior foramina of the *nervi hypoglossi*: the smaller less than a half of the diameter of the larger (0); smaller half or more of the diameter of the larger (1) Fig 12.
3. Anterior process on prootic intruding into the foramen trigemini: absent (0); present (1). Fig. 9.
4. Rostrum basisphenoidale thin, long, and gracile rod: with anterior processes well away from anterior tip of rostrum (0); robust and short rod with anterior processes very close to anterior tip of rostrum (1) . (only applicable if rod shaped) Fig. 11.
5. Labial margin of maxilla: contacts jugal (0); squared off and ends ventral to jugal (1). Fig. 2.
6. Superficial jugal ridge – The superficial jugal ridge is: indistinct, no significant marginal ridge (0); no distinct ridge, but incline along margin, distinguished with texture change (1) ; distinct marginal ridge, distinct textures on either side (2). Fig. 2.
7. Shape of *hiatus accousticus*: opening roughly rectangular from medial view, the ventral portion more than three-quarters the width of the dorsal portion (0) ; differentiation between the two portions much more strongly defined, the ventral portion is half the width of the dorsal portion, the “waist” separating them pinched and narrow (1) . Fig. 9.
8. Posteroventral process of the jugal: absent (0); present, relatively small does not reach posterior to the jugal-quadratojugal margin (Fig. 2E) (1); present, large and extends beyond jugal-quadratojugal margin (2). Fig 2.
9. Extent of the overlap of quadratojugal by jugal: negligible (0); present but minor (1); present, significant overlap (2). Fig 2,

10. Orientation of the surface which provides the origin of the depressor mandibulae from the squamosal: lateral (0), posterior (1). Fig 2.

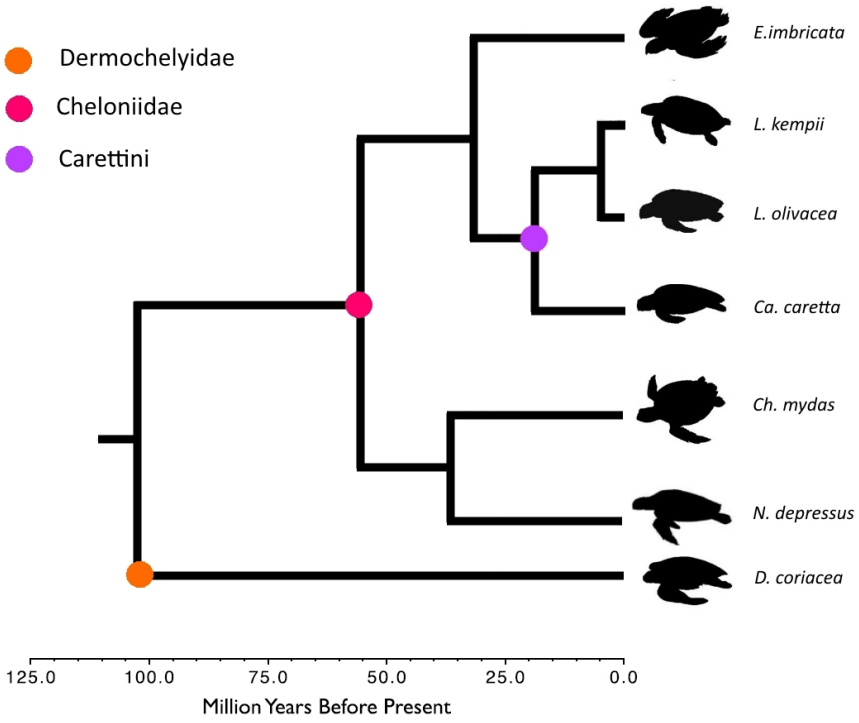

Figure 1. The current consensus for the phylogenetic relationships between extant sea turtles. The different colours represent the base of the groups in extant sea turtles. Redrawn from Duchene et al. (2013). Silhouettes redrawn from Jones et al. (2012).

320x254mm (96 x 96 DPI)

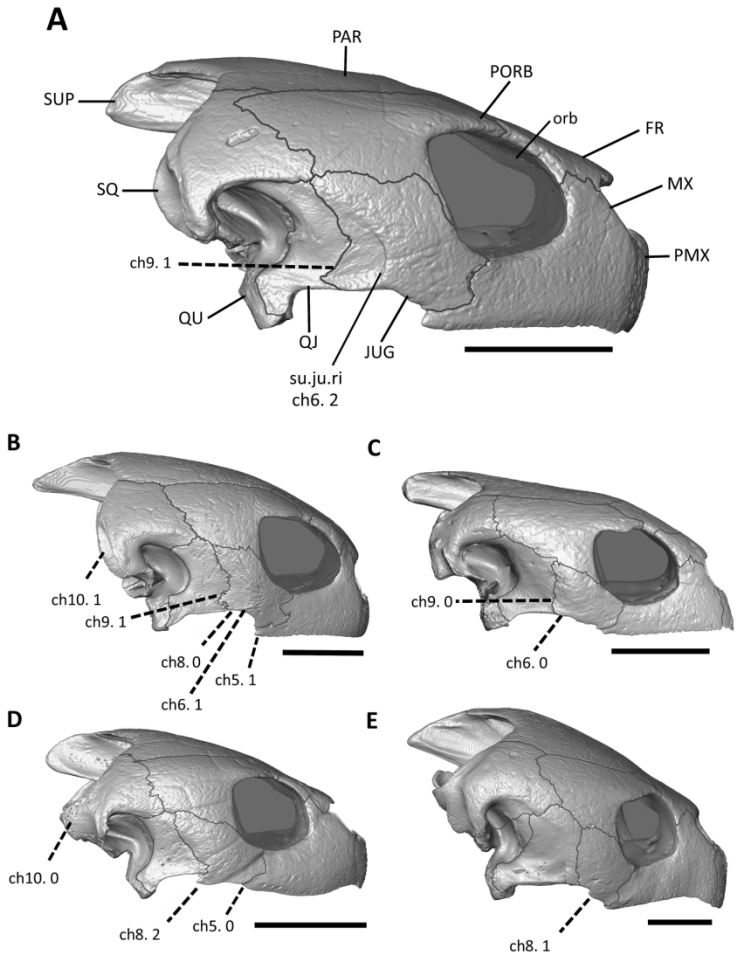

Figure 2. Lateral view of the five genera of extant cheloniid sea turtles. Images are of surface files constructed in Avizo lite 8.0 A *Natator depressus*(WAM R112123). B *Chelonia mydas* (SAMA unregistered). C *Eretmochelys imbricata* (WAM R120113). D *Lepidochelys olivacea* (SAMA BM670). E *Caretta caretta* (SAM Unregistered). Displaying the states of characters 5, 6, 8, 9, 10, based on the descriptors in Appendix 1. Abbreviations: FR, frontal; JUG, jugal; MX, maxilla; orb, orbital opening; PAR, parietal; PMX, premaxilla; PORB, postorbital; PRFR, prefrontal; QJ, quadratojugal; QU, quadrate; SQ, squamosal; su.ju.ri, superficial jugal ridge; SUP, supraoccipital. Scale bars = 50mm

75x107mm (600 x 600 DPI)

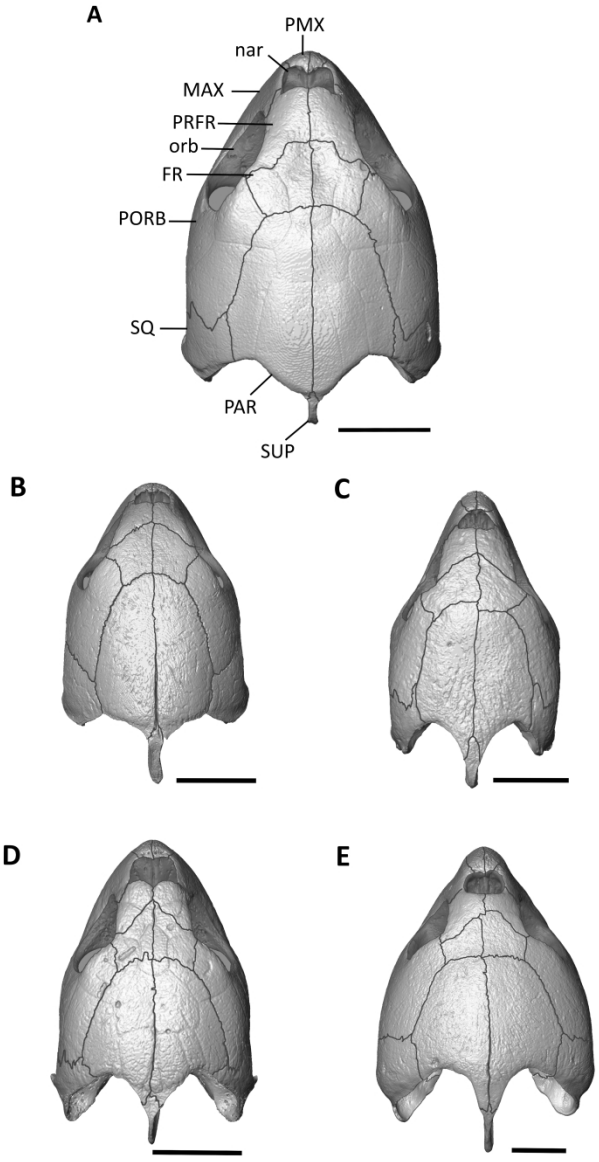

Figure 3. Dorsal view of the five genera of extant cheloniid sea turtles. Images are of surface files constructed in Avizo lite 8.0 A *Natator depressus* (WAM R112123). B *Chelonia mydas* (SAMA unregistered). C *Eretmochelys imbricata* (WAM R120113). D *Lepidochelys olivacea* (SAMA BM670). E *Caretta caretta* (SAM unregistered). Abbreviations: FR, frontal; JUG, jugal; MX, maxilla; nar, Nares; orb, orbital opening; PAR, parietal; PMX, premaxilla; PORB, postorbital; PRFR, prefrontal; SQ, squamosal; SUP, supraoccipital. Scale bar = 50mm

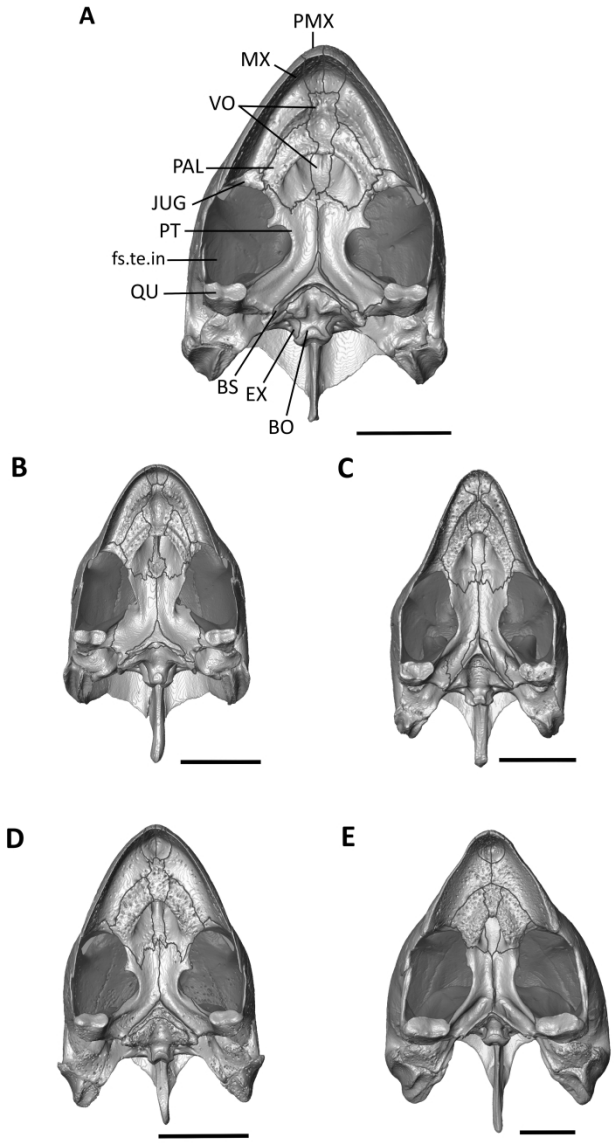

Figure 4. Ventral view of the five genera of extant cheloniid sea turtles. Images are of surface files constructed in Avizo lite 8.0 A *Natator depressus* (WAM R112123). B *Chelonia mydas* (SAMA unregistered). C *Eretmochelys imbricata* (WAM R120113). D *Lepidochelys olivacea* (SAMA BM670). E *Caretta caretta* (SAM unregistered). Abbreviations: BO, Basioccipital; BS, basisphenoid; EX, exoccipital; fo.te.in, fossa temporalis inferior; JUG, jugal; MX, maxilla; PAL, palatine; PMX, premaxilla, PT, pterygoid; QU, quadrate; VO, vomer. Scale bar = 50mm

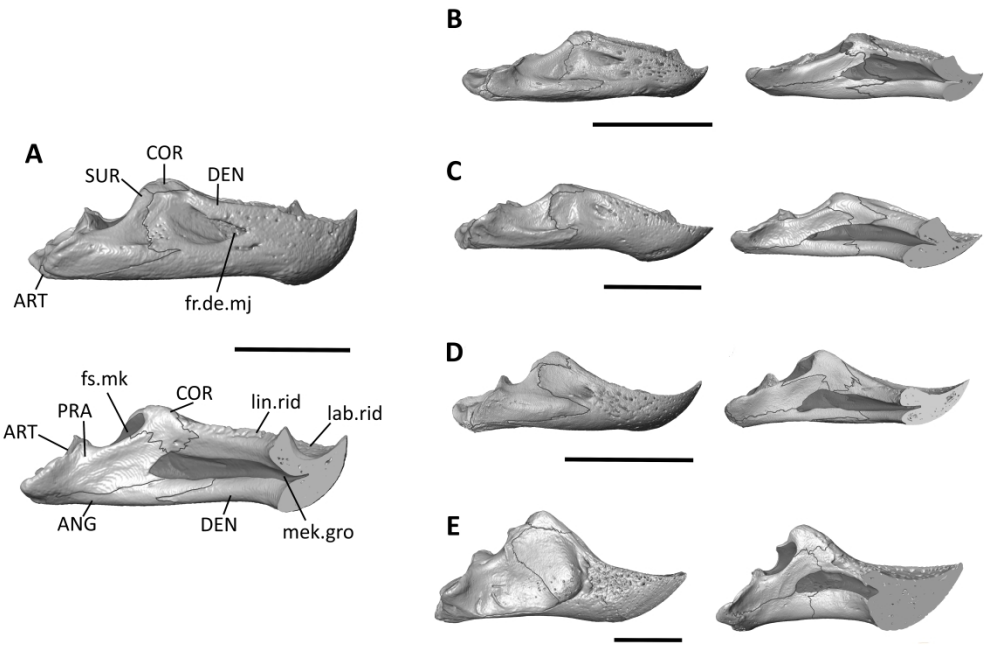

Figure 6. Lateral and medial view of the five genera of the mandibles extant cheloniid sea turtles. Images are of surface files constructed in Avizo lite 8.0 A *Natator depressus* (WAM R112123). B *Chelonia mydas* (NHMUK 1969.776) C *Eretmochelys imbricata* (WAM R120113). D *Lepidochelys olivacea* (SMNS 11070). E *Caretta caretta* (SAM unregistered). Abbreviations: ANG, angular; ART, articular; COR, coranoid; DEN, dentary; for.dent.maj, foramen dento faciale majus; fs.mk, fossa Makelii; lb.rid, labial ridge; lin.ridge; lingual ridge; mek.gro, Mekelian groove; PRA, prearticular; SUR, surangular. Scale bar = 50mm

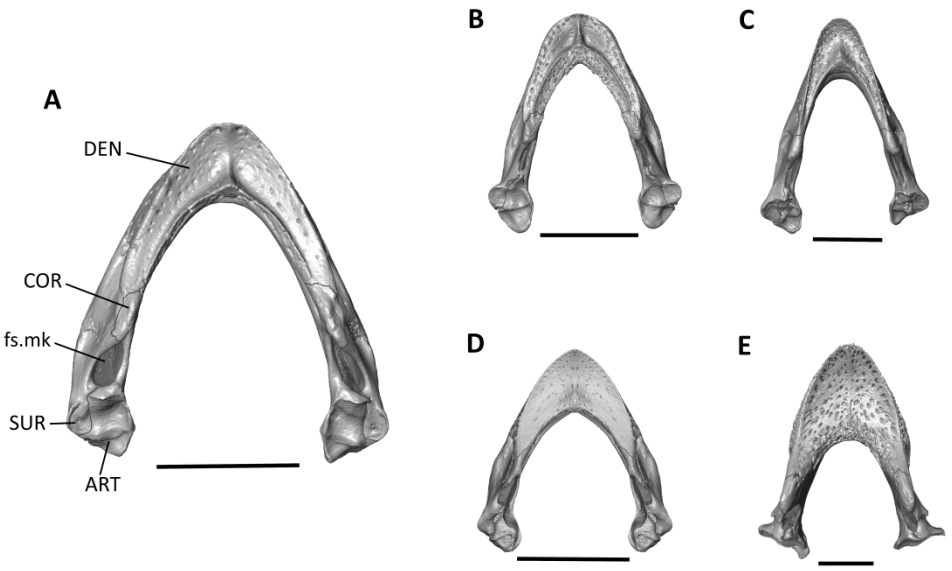

Figure 7. Dorsal view of the mandibles of the five extant extant cheloniid sea turtles. Images are of surface files constructed in Avizo lite 8.0 A *Natator depressus* (WAM R112123). B *Chelonia mydas* (NHMUK 1969.776) C *Eretmochelys imbricata* (WAM R120113). D *Lepidochelys olivacea* (SMNS 11070). E *Caretta caretta* (SAM unregistered). Abbreviations: ANG, angular; ART, articular; COR, coronoid; DEN, dentary; fs.mk, fossa Makelii; Scale bar = 50mm.

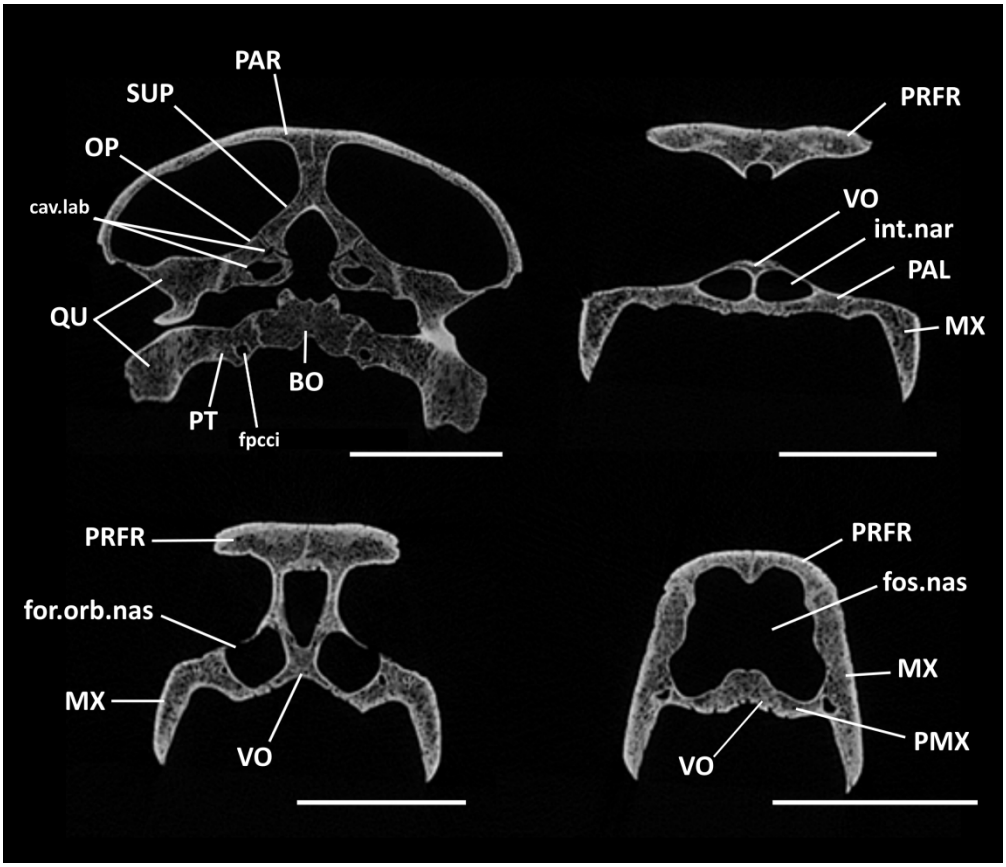

Figure 8. Transverse cross sections *Natator depressus* (WAM R120113) cranium of the posterior portion of the skull (A) and of the nasal region moving anteriorly (B-C). Abbreviations: BO, basioccipital; cav.lab, cavum labrinthicum; fpcci, foramen posterior canalis cartotici interni; fos. nar, fossa nasalis; fos.orb.nas., fossa orbito-nasalis; int.nar., internal nares; MX, maxilla; OP, opsithotic; PAL, palatine; PAR, parietal; PRFR, prefrontal; PT, pterygoid; PT, pterygoid; VO, vomer. Scale bars are 50mm.

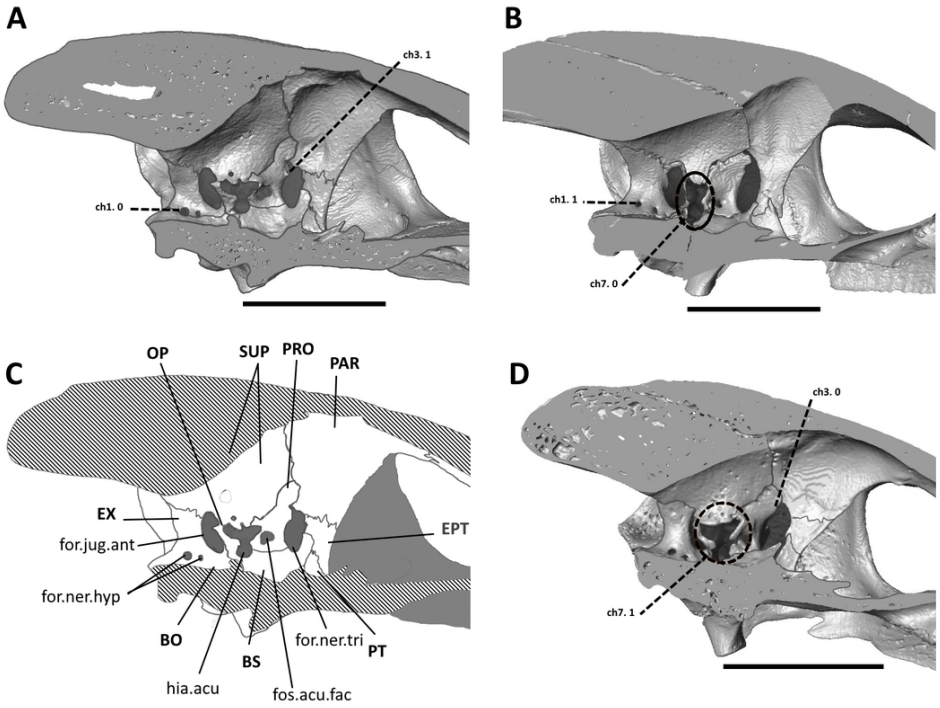

Figure 9. Parasagital cross section of *Natator depressus* (WAM R112123) (A,D) skull, exposing the lateral wall of the braincase. B and C represent the lateral wall of the braincase of *Chelonia mydas* (SAMA Unregistered) and *Lepidochelys olivacea* (SAMA BM670) respectively. A: the original surface file, B: the surface file redrawn and labelled. Areas which are "cut through" are shaded with diagonal lines. Displaying the states of characters 1, 3, 7, based on the descriptors in Appendix 1. Abbreviations: BO, basioccipital; BS, basisphenoid; EPT, epipterygoid; EX, exoccipital; for.ner.hyp., foramen nervi hypoglossi; for.ner.tri., foramen nervi trigemini; for.jug.ant.,foramen jugulare anterius; hia.acu., hiatus acousticus; OP, opisthotic; PAR, parietal; PT, pterygoid; PRO, prootic: SUP, supraoccipital. Scale bars = 20mm

47x34mm (600 x 600 DPI)

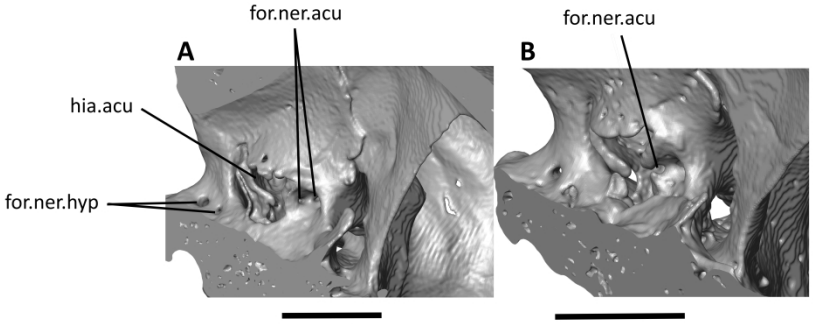

Figure 10. Antero-medial view of brain case of *Natator depressus* (WAM R112123) (A) and *Lepidochelys olivacea* (SAMA BM670). (B) showing the closed (A) and open (B) states of the medial foramen nervi acustici. Abbreviations: for.ner.ac, foramen nervi acustici; for.ner.hy, foramen nervi hypoglossi; hia.acu, hiatus acusticus. Scale bars = 20mm

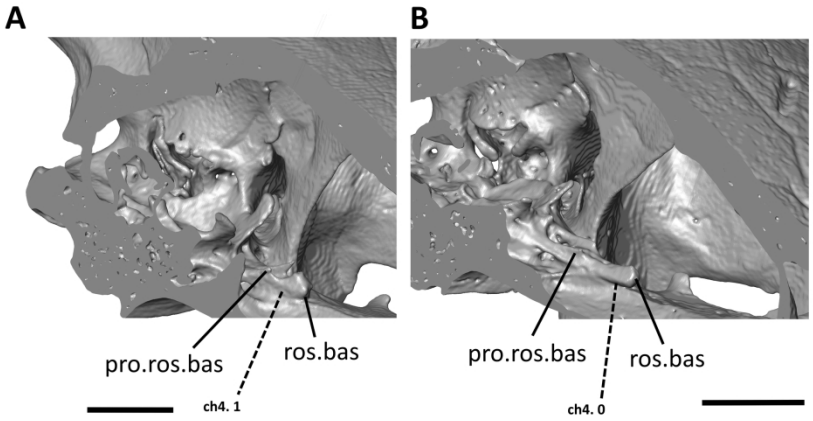

Figure 11. Antero-medial view of brain case of *Natator depressus* (WAM R112123) (A) and *Lepidochelys olivacea* (SAMA BM670). (B) illustrating the two states of the *rostrum basisphenoidale*, robust (A) and gracile (B). Displaying the states of character 4 based on the descriptor in Appendix 1. Abbreviations: pro.ros.nas processus rostrum basisphenoidale; ros.bas, rostrum basisphenoidale. Scale bars = 20mm

121x83mm (600 x 600 DPI)

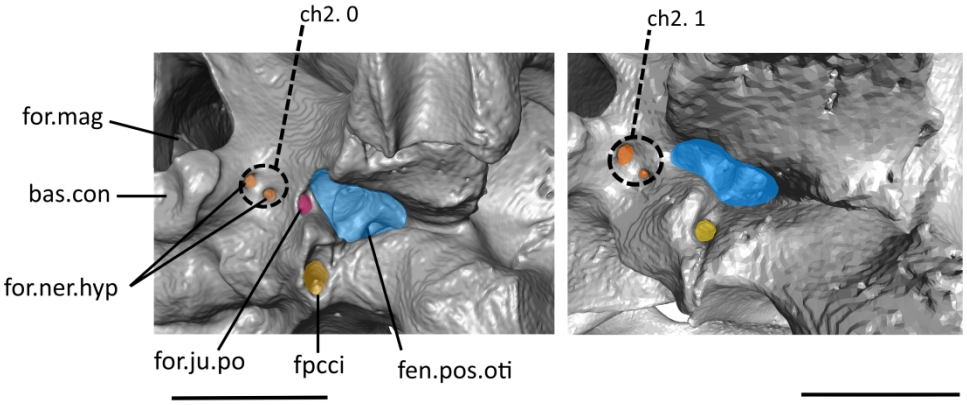

Figure 12. Ventro-posterior-lateral view of *Natator depressus* (WAM R112123) (A) to highlight the foramen jugulare posterious, and *Eretmochelys imbricata* (WAM R120113) (B) for comparison. Displaying the states of character 2 based on the descriptor in Appendix 1. Abbreviations: bas.con, basioccipital condyle; fn.po, fenestra postotica; for.ju.po, foramen jugulare posterious; for.mag, foramen magnum; for.ner.hyp, foramen nervi hypoglossi; fpcci, foramen posterior canalis cartotici. Scale bars = 20mm

1404x650mm (96 x 96 DPI)

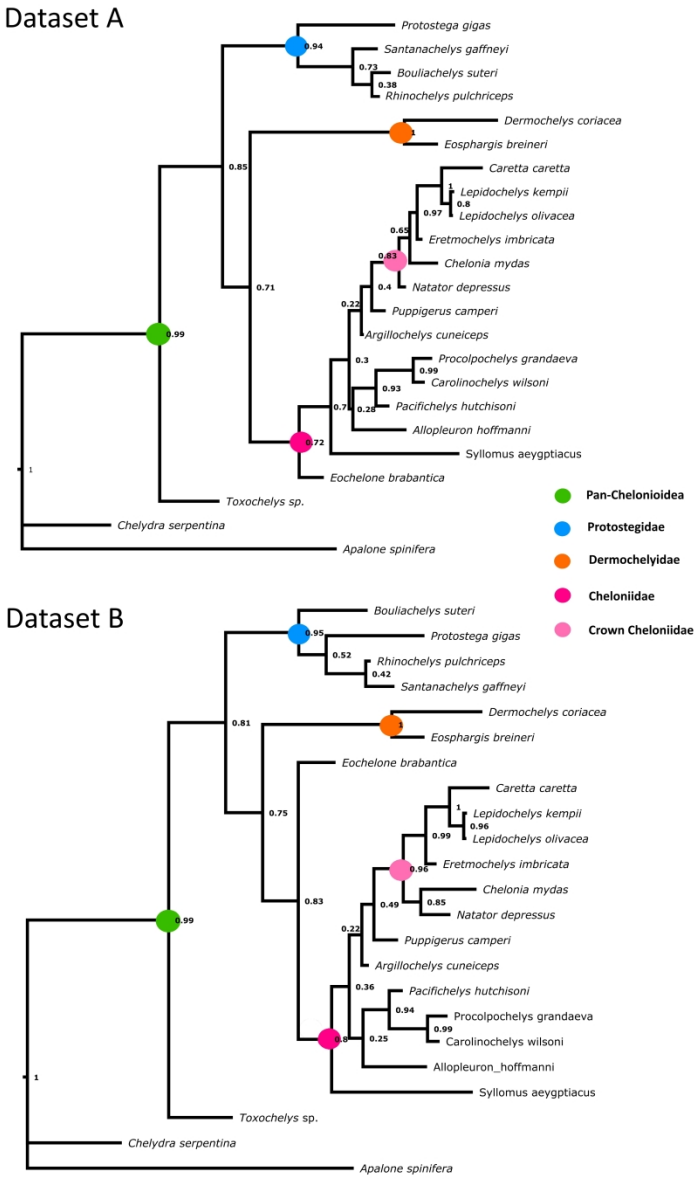

Figure 13. Maximum credibility Bayesian trees. Dataset A based on the matrix from Evers and Benson (2019). Dataset B based on matrix from Evers and Benson (2019) with added characters found in this study. Different colours at nodes represent base of clades. Numbers at the node show posterior probability value of node.

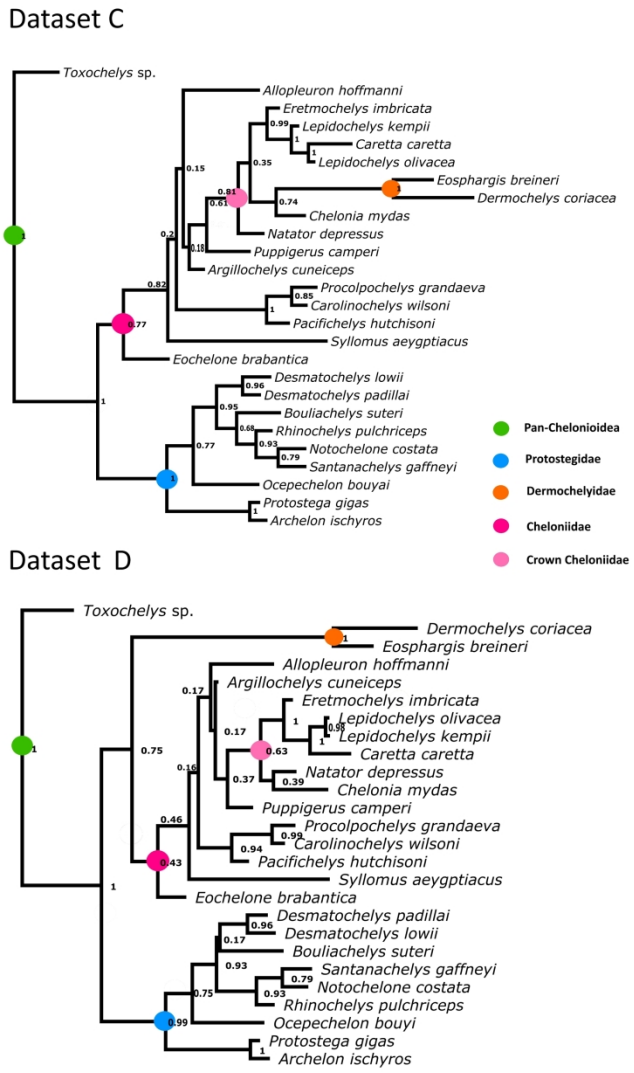

Pruned maximum credibility Bayesian trees. Dataset C based on the matrix from Evers and Benson (2019). Dataset D based on matrix from Evers and Benson (2019) with added characters found in this study. Colours at nodes represent base of clades. Numbers at the node show posterior probability value of node.

117x158mm (600 x 600 DPI)